Proceedings of

SPHERIC 2017

12th International SPHERIC Workshop

Ourense, 13 - 15 June 2017

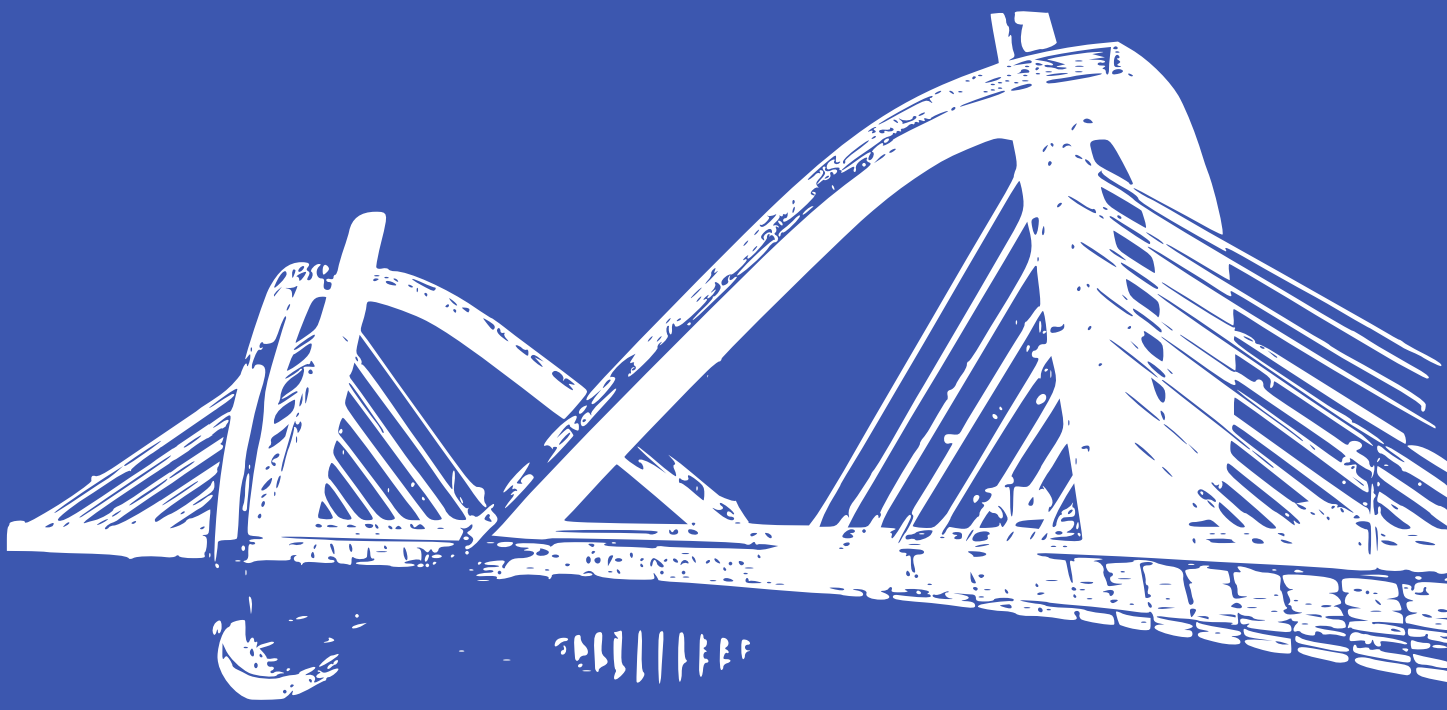

Universidade Vigo

Flanders Hydraulics Research

Flanders State of the Art

Facultade de Ciencias
Universidade Vigo

Escola de Enxeñaría Aeronáutica e do Espazo
Universidade Vigo

Environmental | Physics | Laboratory
EPhysLab

spheric
ERCOFTAC

Proceedings of the 12th International SPHERIC Workshop

Ourense, 13-15 June 2017
Universidade de Vigo, Spain

ISBN: 978-84-697-3678-4

Organised by
Universidade de Vigo
Flanders Hydraulics Research

Edited by
Alejandro J. C. Crespo
Moncho Gómez Gesteira
Corrado Altomare

Targeting viscous flows around solid body at high Reynolds numbers with the δ *plus*-SPH model

P.N. Sun, A.M. Zhang
College of Shipbuilding Engineering,
Harbin Engineering University,
Harbin, China
sunpengnan@hrbeu.edu.cn

A. Colagrossi, S. Marrone, M. Antuono
CNR-INSEAN
Marine Technology Research Institute, 00128 Rome, Italy
andrea.colagrossi@cnr.it

***Abstract*—To avoid the inception of tensile instability, the δ^+-SPH scheme is modified by switching the momentum equation to a non-conservative formulation in those fluid regions characterized by negative pressure. The loss of conservation properties is shown to induce small errors, provided that the particle distribution is regular. The latter condition is ensured by implementing the Particle Shifting Technique (PST). The novel variant of the δ^+-SPH is proved to be effective in preventing the onset of tensile instability in a number of challenging benchmark tests, as for example, flows past bluff bodies at high Reynolds numbers. Reference solutions for the benchmark cases are obtained through DVH and Navier-Stokes solvers. A final simulation characterized by a deforming body that resembles a fish-like swimming is used as a practical application of the δ^+-SPH model in biological fluid mechanics.**

I. Introduction

The modelling of boundary layers through classical SPH models is generally a challenging problem because of the irregular particle distribution induced by large velocity gradients. The above problem worsens when the occurrence of negative pressure regions leads to the onset of the so-called tensile instability, causing the generation of voids inside the computational fluid domain. For these reasons, the attainment and maintenance of a regular particle distribution is of crucial importance during the flow evolution. Recently, different algorithms have been proposed to measure (e.g. [1]) or reduce the particle disorder (e.g. Particle Packing Algorithm [2], Particle Shifting Technique (PST) [3], the Dynamic Stabilization (DS) [4, 5]) both in weakly-compressible or incompressible SPH models. Despite the good performances of these algorithms at low and moderate shear stresses, their extension to flows characterized by intense velocity gradients, as for example the flow past a bluff body at high Reynolds numbers, still remains a challenging problem.

In the SPH literature there are well-established strategies for simulating flows around simple geometries (e.g. circular cylinder) for Reynolds numbers in the regime $Re \in [1, 1000]$, see e.g. [6]. For weakly-compressible SPH models, a background pressure is generally needed in order to avoid the onset of tensile instability in the wake region (where negative pressure occurs). In fact, this expedient requires an accurate calibration and can limit the application of the model to more general problems (e.g. free-surface flows). An alternative strategy to the use of the background pressure is the Particle Shifting Technique (PST), which relies on the addition of a suitable shifting velocity to the Lagrangian velocity of particles. This approach also allows for a more regular particle distribution and for an improved evaluation of the velocity gradients (e.g. vorticity). The application of the PST to the δ-SPH scheme (see [7, 8]) is at the basis of the δ^+-SPH scheme [9].

Despite the good performances of the δ^+-SPH scheme, the tensile instability still represents a major problem as the Reynolds number increases and a more thorough understanding of its genesis is required to get rid of this phenomenon. With respect to this, the cause of the tensile instability has to be pursued in the structure of the SPH pressure gradient. As highlighted in [2], when the pressure field is positive, the pressure gradient contains a stabilizing term which leads to the particle resettlement towards ordered and uniform distributions. On the contrary, when the pressure field becomes negative, such a term behaves in the opposite way, causing particles to cluster and leading to the generation of voids in the computational fluid domain.

In the present work, we show that a simple strategy to avoid this problem is achieved by switching to a non-conservative formulation of the pressure gradient in the negative pressure regions. This is equivalent to neglect the term that causes the particle resettlement (and, therefore, the tensile instability). The loss of the conservation properties induces only limited errors, provided that the particle distribution remains regular (see [1]). This latter point is easily achieved thanks to the Particle Shifting Technique (see, for example, [3, 9]).

The proposed variant of the δ^+-SPH is tested against a number of challenging benchmark problems and is compared with the numerical solutions obtained by using classic Navier-Stokes solvers and the Diffused Vortex Hydrodynamics (DVH) method (see [10]). The present work is arranged as follows: in Section II, the SPH methodology is introduced along with details on the theoretical aspects on the tensile instability phenomenon, while in Section III an in-depth validation of the proposed model is performed.

II. SPH Methodology

The δ^+-SPH belongs to the class of weakly-compressible SPH schemes, that is, those SPH solvers that rely on the hypothesis that the fluid is weakly compressible and barotropic. Specifically, a linear state equation is assumed between the pressure and the density field. For computational reasons (see [11]), the sound velocity, c_0, is usually chosen according to the following bound:

$$c_0 \geq 10 \max\Big(U_{max}, \sqrt{p_{max}/\rho_0} \Big) , \tag{1}$$

where U_{max} and p_{max} are the maximum expected velocity and pressure. This ensures that the density variations are below 1%, in agreement with the weakly compressibility hypothesis.

Similarly to the δ-SPH scheme (from which it derives), the δ^+-SPH scheme contains a numerical diffusive term inside the continuity equation which helps reducing the high-frequency oscillations that usually affects the pressure field as a consequence of the weakly compressibility assumption. The governing equations for the δ^+-SPH scheme are:

$$\begin{cases} \dfrac{\mathrm{d}\rho_i}{\mathrm{d}t} = -\rho_i \displaystyle\sum_j V_j (\boldsymbol{u}_j - \boldsymbol{u}_i) \cdot \nabla_i W_{ij} \; + \; \delta\, h\, c_0\, \mathcal{D}_i \\ \dfrac{\mathrm{d}\boldsymbol{u}_i}{\mathrm{d}t} = \boldsymbol{f}_i - \dfrac{1}{\rho_i} \displaystyle\sum_j F\Big(p_j, p_i\Big) \nabla_i W_{ij}\, V_j + \dfrac{\mu}{\rho_i} \displaystyle\sum_j \pi_{ij} \nabla_i W_{ij}\, V_j \\ \dfrac{\mathrm{d}\boldsymbol{r}_i}{\mathrm{d}t} = \boldsymbol{u}_i \,, \qquad p_i = c_0^2 (\rho_i - \rho_0) \,, \qquad \boldsymbol{r}_i^* = \boldsymbol{r}_i \; + \; \delta \boldsymbol{r}_i \,, \end{cases} \tag{2}$$

where $\mathrm{d}/\mathrm{d}t$ denotes the material derivation with respect to time. The first three equations are respectively the continuity, momentum and advection equations. Symbols $\boldsymbol{r}_i$ and $\boldsymbol{u}_i$ indicate the position and the velocity of the i-th particle while $\boldsymbol{r}^*$ is the modified position after the particle shifting $\delta\boldsymbol{r}$ is applied (more details will be given later). The particle mass, m_i, is maintained constant during the simulation, this ensuring the mass conservation of the overall fluid phase, while the particle volume is $V_i = m_i/\rho_i$. Finally, $\boldsymbol{f}_i$ is a generic the body force and μ is the dynamic viscosity.

In the present work the kernel function W_{ij} is a $C2$ Wendland kernel (see [12]) with smoothing length h, that is set equal to $2\Delta x$ where Δx is the initial particle distance. This corresponds approximately to 50 particles in the kernel support.

The viscous term in system (2) is represented following [13]. The diffusive term is the same used in the δ-SPH scheme. As a common practice the diffusive parameter δ is set equal to 0.1 (see [8, 14]).

Finally, we focus on the pressure gradient argument $F_{ji} = F(p_j, p_i)$. Generally, under the weakly compressibility assumption, this term is represented by $(p_j + p_i)$ (or by an equivalent sum of terms depending on pressure and density) and the differential operator can be split in the following manner:

$$\sum_j \Big(p_j + p_i\Big) \nabla_i W_{ij}\, V_j \; = \; \sum_j \Big(p_j - p_i\Big) \nabla_i W_{ij}\, V_j \; + \; 2\, p_i \sum_j \nabla_i W_{ij}\, V_j \,. \tag{3}$$

As shown in [15], the first term in the right-hand side is the smoothed counterpart of the actual pressure gradient. When the pressure field is positive (i.e. $p_i \geq 0$), the last term in the right-hand side behaves as a regularizing internal force and leads to the particle resettlement towards uniform spatial configurations. This property has been used, for example, in [2] to build a particle packing algorithm for the initial particle positioning in complex geometries. On the contrary, if the pressure field is negative, the last term in equation (3) behaves in the opposite way, increasing the particle disorder and eventually leading to the occurrence of voids regions in the computational domain. A naive way to get rid of this issue is to drop such a term when the pressure becomes negative. Unfortunately, this leads to problems close to the free surface where the pressure generally oscillates around the zero value. A more robust strategy is to maintain the second term in the right-hand side of equation (3) when the fluid particles are close to the interface. This corresponds to:

$$F_{ji} \; = \; \begin{cases} p_j + p_i & p_i \geq 0 \quad \text{or} \quad i \in \mathscr{S}_F \\ p_j - p_i & p_i < 0 \quad \text{and} \quad i \notin \mathscr{S}_F \end{cases} \tag{4}$$

where $\mathscr{S}_F$ denotes the region of the fluid domain close to the free surface, that is the free-surface particles and their neighbour particles. The free surface particles are detected through the algorithm described in [16].

The main drawback related to the use of the switch in equation (4) is the loss of conservation of linear and angular momenta when the negative sign is applied. Furthermore, the switch also lessens the robustness of the SPH scheme (see e.g. [17]). The above issues are, however, reduced by implementing the Particle Shifting Technique, this helping maintaining a regular and homogeneous particle distribution all over the computational domain. The shifting displacement is given by:

$$\delta \boldsymbol{r}_i \; = \; -\mathit{CFL}\, \frac{U_{max}}{c_0}\, (2h)^2 \sum_j \left[1 \; + \; R \left(\frac{W_{ij}}{W(\Delta x)} \right)^n \right] \nabla_i W_{ij}\, \frac{m_j}{\rho_i + \rho_j} \,,$$

where $n = 4$, $R = 0.2$ and CFL is the Courant-Friedrichs-Levy number (here set equal to 1.5). In particular, a fourth-order Runge-Kutta scheme is used to march in time the system (2). In order to reduce CPU costs and improve the stability of the scheme, the particle repositioning is applied outside the sub-time steps of the Runge-Kutta scheme, as described in [9].

III. Applications

In this section we show some practical $2D$ applications of the proposed variant of the δ^+-SPH scheme. Specifically, we focus on flows past: a NACA profile, a circular cylinder and a deforming body. All the body profiles are inside a rectangular channel with an inflow condition on the left wall

and an outflow condition on the opposite side. This requires the implementation of different boundary condition along the solids. Specifically:

1) Free-slip boundary conditions are implemented on the lateral walls of the channel by using Fixed Ghost Boundaries as in [18],
2) No-slip boundary conditions are implemented on the body surfaces by using Fixed Ghost Boundaries and an asymmetric extension of the tangential velocity (ASM) (see [6, 19])
3) Inflow and outflow boundaries are implemented as described in [18],

With respect to the last point, a major issue is related to the expulsion of the strong vortices generated by the solid structures out of the fluid domain. To obtain a reliable outflow condition, a buffer damping zone with a width of $5L$ (where L is the characteristic length of the bluff body) is attached to the outflow boundary. In this region the viscosity coefficient is increased to obtain $Re \in [1, 10]$ in order to regularize the flow before the outflow boundary.

In all the simulations the particle positions are initially set by using the particle packing technique described in [2]. In order to properly resolve the boundary layer regions, in all the simulations an Adaptive Particle Resolution (APR) method has been implemented (for details see [20]). Validations are carried out by comparing the vorticity field and the coefficients related to pressure, drag and lift force acting on the body with reference solutions. Specifically, these are defined as follows:

$$C_p = \frac{2\,p}{\rho U^2 L}, \qquad C_D = \frac{2\,f_D}{\rho U^2 L}, \qquad C_L = \frac{2\,f_L}{\rho U^2 L}, \tag{5}$$

where f_D and f_L denote the drag and lift force measured on the body following the procedure described in [6, 21].

A. Flow past a NACA0010 profile at $Re = 10,000$ and with angle of attack $\alpha = 30°$

In this section, we consider the flow past a stationary NACA0010 profile at $Re = 10,000$ and angle of attack $\alpha = 30°$. The computational domain is $[-8L, 22L] \times [-8L, 8L]$ (here L indicates the airfoil chord) and the body center is located at the origin of the frame of reference. The maximum particle resolution is $L/\Delta x = 400$ and 5 levels of particle refinements are used (for details see [9]) so that $L/\Delta x = 25$ far from the body.

The chosen Reynolds number and angle of attack rapidly lead to the vortex detachment on the leading and trailing edges of the NACA profile and, consequently, the present simulation allows us to test the Tensile Instability Control (TIC) proposed in section §II. In Figure 1 some snapshots of the numerical results obtained with and without the TIC are displayed. In the former case, large void regions are generated after few instants from the beginning of the simulation and merge together and grow as the simulation advances in time. On the contrary, the use of the TIC completely eliminate the occurrence of tensile instability and allows for a physical development of the boundary layer and consequent vortex shedding.

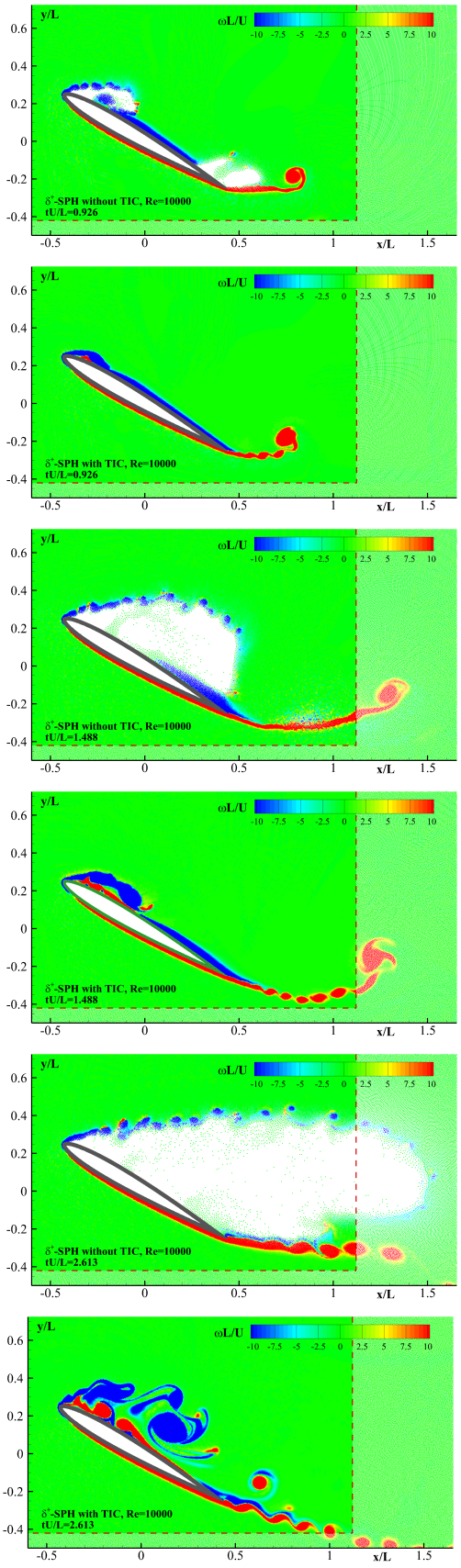

Fig. 1. Snapshots of the flow around a NACA0010 profile at $Re = 10,000$ using the δ^+-SPH model without and with Tensile Instability Control.

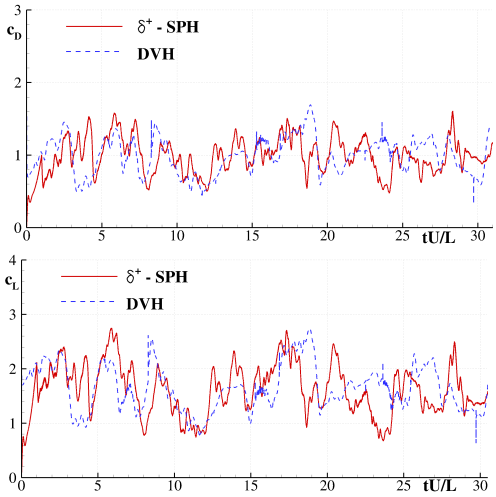

Fig. 2. Drag (top) and lift (bottom) coefficients for the NACA0010 profile at $Re = 10,000$. Comparison between the present δ^+-SPH scheme and the DVH [10]

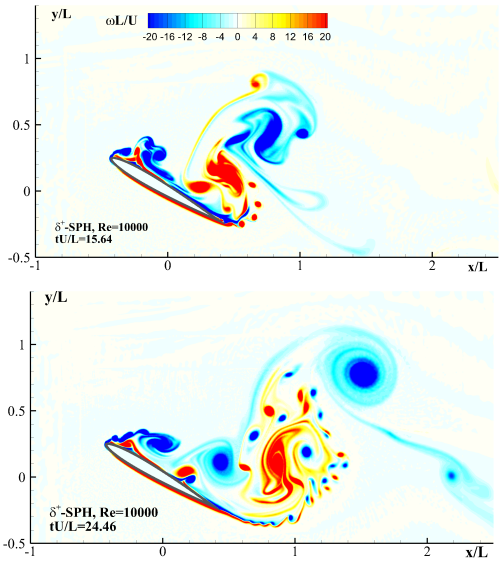

Fig. 3. Details of the vorticity distribution close to the foil at two time instants.

A validation for this case is carried out by comparing the drag and lift force coefficients predicted by the δ^+-SPH and DVH results. As shown in Figure 2 a similar behaviour is observed for both the coefficients.

The pressure gradient near the trailing edge makes the secondary vortices to roll up and interact with the eddies developed from the leading edge and the suction side. A detailed view of the vorticity distributions close to the body at $tU/D = 15.64$ and $tU/D = 24.46$ is shown in Figure 3.

Finally, Figure 4 shows the pressure field (with an opposite sign) around the solid body at $tU/L = 7.488$. Accordingly, the peaks indicates the points in which the pressure attains large negative values. These peaks are not close to the NACA0010 profile but are generally located at the core of the strong

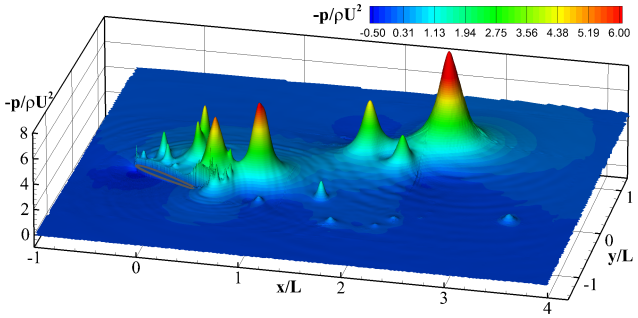

Fig. 4. The pressure field at $tU/L = 7.488$.

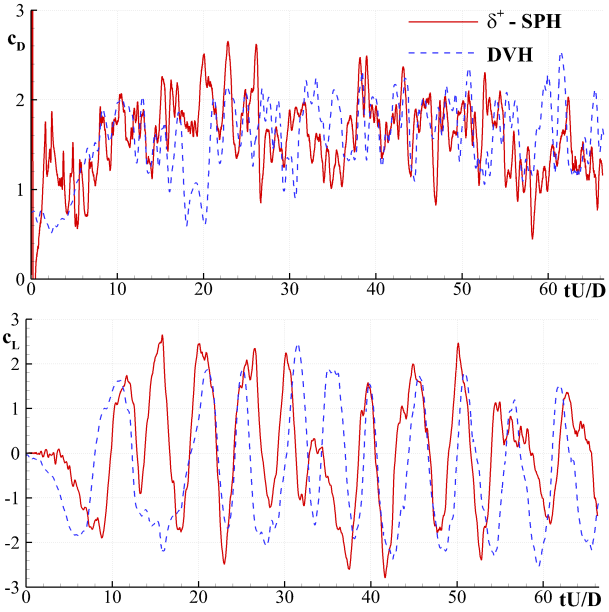

Fig. 5. Flow past a circular cylinder at $Re = 9500$: time histories of the drag (top) and lift (bottom) coefficients as predicted by the δ^+-SPH and DVH.

vortical structures. This result further shows the ability of the proposed variant of the δ^+-SPH model to prevent the tensile instability.

B. *Flow past a circular cylinder at Re* = 9500

In the present section the flow past a circular cylinder at $Re = 9500$ is considered. This corresponds to the lower sub-critical regime for this kind of problem and is characterized by an unstable boundary layer and by a chain of eddies that are formed in the shear layer and are transported downstream into the vortex wake (see, for example, [22]). The computational domain is $[-8D, 22D] \times [-8D, 8D]$ and the body is located at the origin of the frame of reference. Five levels of refinement are used and the spatial resolution close to the cylinder is $D/\Delta x = 400$, this corresponding to about $1,450,000$ particles in the whole fluid domain. It is worth noting that without the spatial refinement the total number of particles would be about $76,800,000$, that is about 50 times larger.

A primary validation of the δ^+-SPH model is carried out by comparing the drag and lift coefficients with those predicted through the DVH method (see figure 5). Both schemes predict

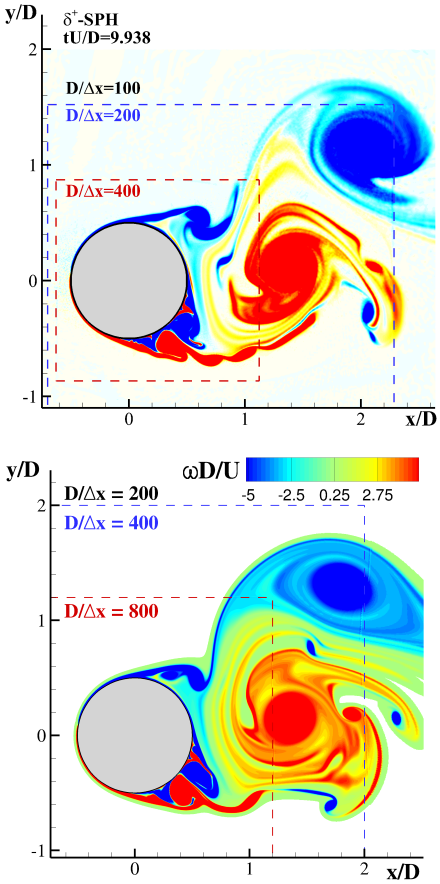

Fig. 6. Flow past a circular cylinder at Re = 9500: vorticity field as predicted by the δ^+-SPH (top) and DVH (bottom).

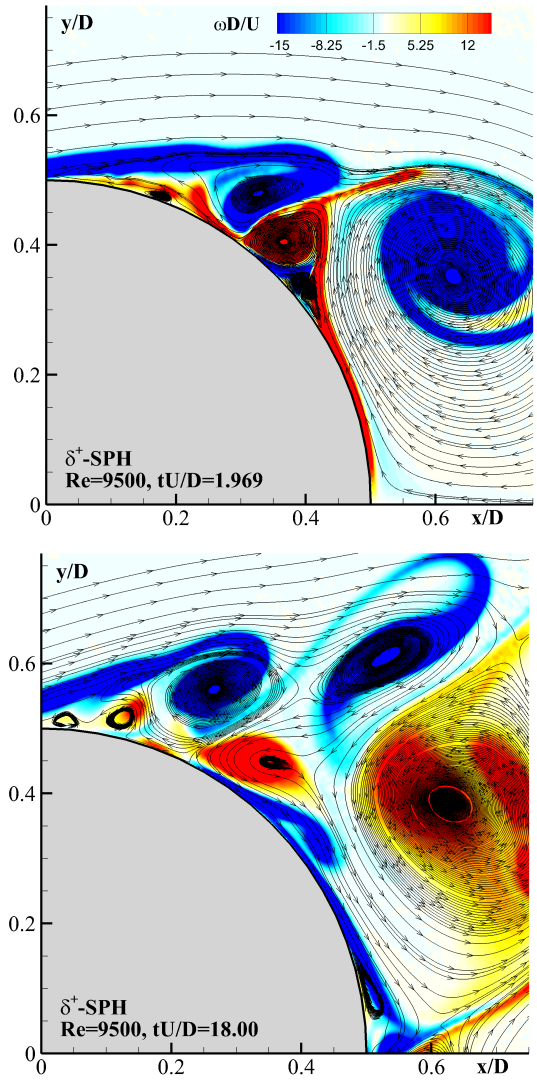

Fig. 7. Flow past a circular cylinder at Re = 9500: details of the vorticity field and streamlines as predicted by the δ^+-SPH.

an almost chaotic behaviour of C_D and C_L because of the unstable boundary layer. In any case, the mean values and the amplitude of the oscillations of these coefficients are approximately the same in both the schemes. The comparison for the vorticity field close to the cylinder is displayed in figure 6 at tU/D = 9.938. Despite the spatial resolution of the δ^+-SPH is half the resolution of the DVH method, the agreement is still satisfactory.

A more in-depth analysis of the mechanism of vorticity generation can be drawn by observing an enlarged view of the boundary layer close to the cylinder. Figure 7 shows two snapshots of the vorticity field at tU/D = 1.969 and tU/D = 18.00. At tU/D = 1.969, two shear layers merge together in the upper shoulder of the cylinder and form a "λ-shape" vortex structure. This separates two vortices of negative vorticity: the smallest one is close to the λ-shape vortex while the largest one starts detaching from the solid body. At tU/D = 18.00, the vortex wake is fully developed and several vortex structures are generated by the boundary layer separation. The overall distribution is almost chaotic and is typical of the sub-critical regime.

C. *Fish-like swimming modelling*

As a final problem, we consider the motion of a deformable body resembling a fish-like swimming model. The equilibrium configuration for this body is represented through a 2D NACA0012 profile so that the middle-line of the foil describes the backbone of a fish. As the middle-line undergoes a transversal motion in the form of waves propagating in the streamwise direction, the movement of the backbone of a fish is mimicked. Following [23], the evolution of the middle-line are described through:

$$y_m = A_m(x_m)\cos(2\pi(x_m - c\,t) + \phi) \qquad (6)$$

where $x_m/L \in [0,1]$ is the horizontal coordinate (from foil head in the streamwise direction), and y_m denotes the movement of the middle-line of the NACA0012 foil in the transversal direction. As usual, L is the length of the fish model while c is the phase speed of the wave propagation (here set

to $2\,m/s$) and ϕ is a phase shift (here set to zero without any loss of generality). The amplitude of the waving motion is represented through a quadratic polynomial as follows:

$$A_m\,(x_m) \;=\; C_0 \;+\; C_1\,x_m \;+\; C_2\,x_m^2\,. \qquad (7)$$

Following [24], we set $C_0 = 0.02$, $C_1 = -0.0825$ and $C_2 = 0.1625$ in order to simulate a saithe swimming motion.

An inflow velocity U is imposed at the left side of the computational domain and the Reynolds number is set equal to $Re = \rho UL/\mu = 5000$. The foil is stationary except for the waving motion. When the drag force measured along the foil is negative, the "fish" swims forward thanks to the propulsion generated by the waving motion. The computational domain is $[-2L, 8L] \times [-4L, 4L]$ and the center of the body is located at origin of the frame of reference. The spatial resolution is $L/\Delta x = 400$ close to the body and in the wake region while decreases to $L/\Delta x = 50$ far from it (specifically, four levels of refinements have been used).

The pressure and vorticity distributions around the waving foil at four time instants $t/T = 0, 0.25, 0.5$ and 0.75 are depicted in Figure 8. Strong negative pressure values are observed at the cores of the vortices while large negative pressure regions alternate along the upper and lower sides of the foil during its motion. These mainly contributes to the generation of a thrust force that propels the foil forward.

The LCSs around the foil are depicted in Figure 9. The drag and lift force coefficients are measured in the SPH simulation and compared to the results of a FEM Navier-Stokes solver [23] in Figure 10. A good agreement is observed between δ^+-SPH and FEM. Both the simulations show a negative drag force on the foil, which means that with a phase speed of $c = 2.0$ the "fish" swims forward with a velocity larger than U in a fluid at rest.

The pressure distribution around the waving foil at $t/T = 0$ is also measured. The pressure contribution on the thrust force is defined as $f_{xp} = p \cdot n_x$ where n_x is the component in the streamwise of the unit normal n on foil surface. Again, good agreement is achieved between different solvers, see Figure 11. This shows that a large drag force acts at the head of the foil, while the shaking tail produces major propulsive contributions. Since in this part, the main purpose is to validate the numerical scheme, a case with a single fish is presented and validated. But the numerical scheme can be straightforwardly extended to the simulation of a swimming fish-group and to the investigation of their hydrodynamic interactions.

Conclusions

In the present paper, an enhanced δ^+-SPH model is proposed which allows preventing the onset of tensile instability. This is achieved by switching to a non-conservative formulation when the pressure field becomes negative. The effects related to the loss of conservation of linear and angular momenta are maintained small by implementing the Particle Shifting technique, this helping the attainment of regular particle distributions.

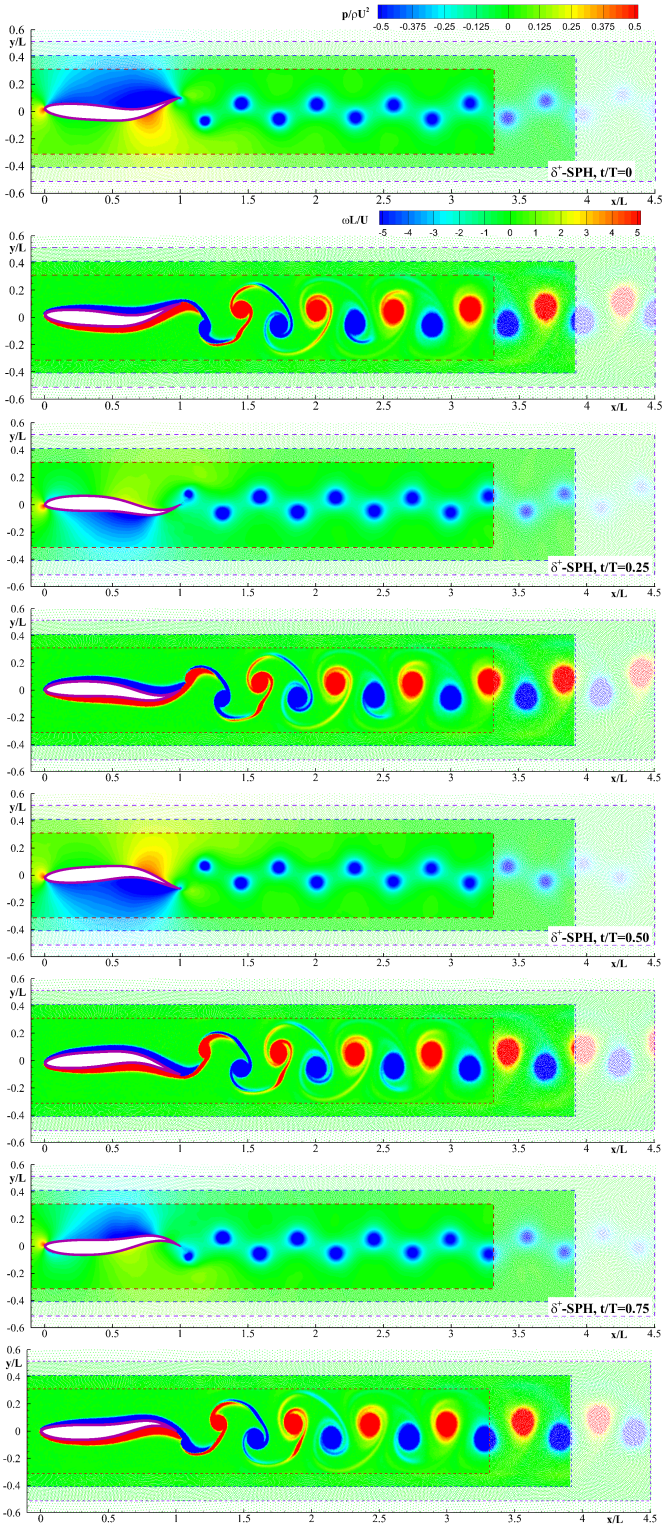

Fig. 8. Fish-like swimming model. Snapshots of the pressure field and vorticity field at different time instants.

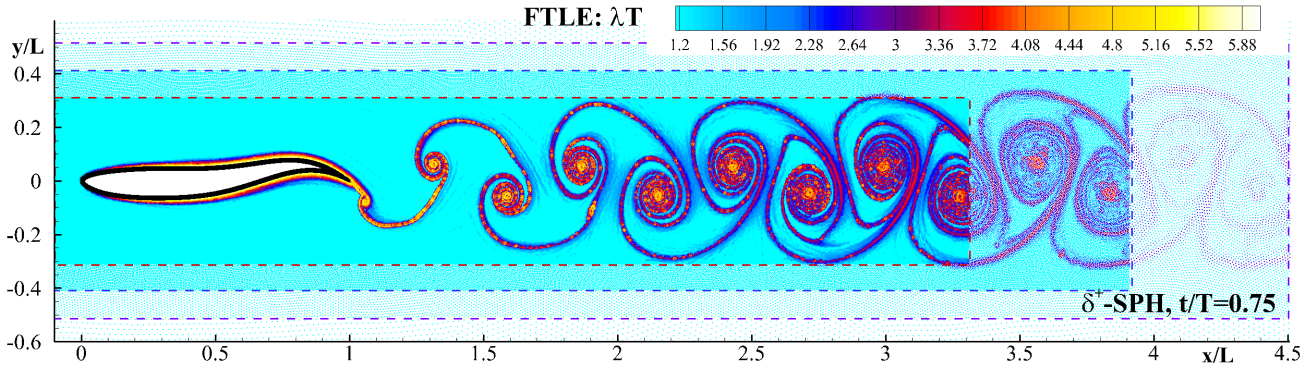

Fig. 9. LCSs in the wake of the fish-like swimming profile

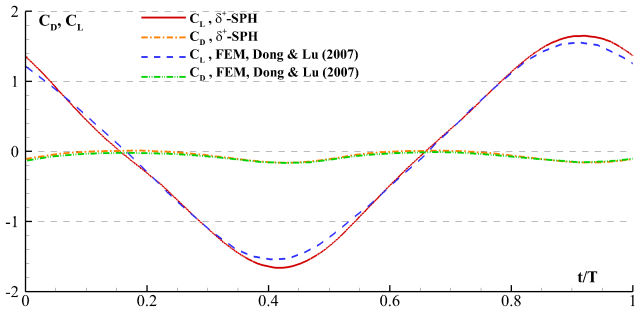

Fig. 10. Fish-like swimming model: the drag and lift force coefficients in one swimming period

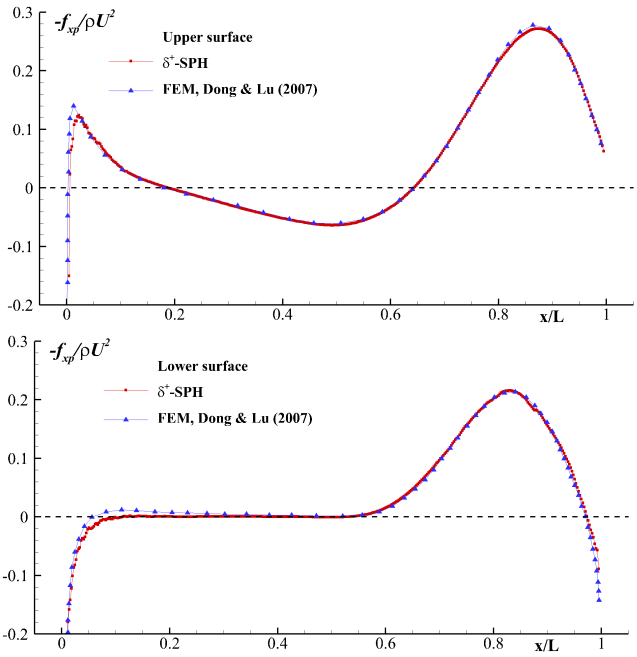

Fig. 11. Fish-like swimming model. Pressure distribution along the upper (top panel) and lower (bottom panel) profiles of the foil surface at $t/T = 0$.

To test the proposed method, Direct Numerical Simulations of flows past airfoils at different angles of attack and past a circular cylinder have been conducted at large Reynolds numbers. All the simulations have been carried on implementing an adaptive particle resolution algorithm. Both fixed and deformable solid profiles have been considered, proving the proposed variant of the δ^+-SPH scheme to be robust and accurate. In particular, the latter test case, mimicking a fish-like swimming motion, suggests that the present scheme may be suitable for applications in biological fluid mechanics.

Acknowledgements

This work is funded by the CNR-INSEAN within the Project PANdA (PArticle methods for Naval Applications, INSEAN Protocol No. 3263, 21 October 2014), the China Scholarship Council (CSC, Grant No. 201606680004) and the National Program for Support of Top-notch Young Professionals.

References

[1] M. Antuono, B. Bouscasse, A. Colagrossi, and S. Marrone, "A measure of spatial disorder in particle methods," *Computer Physics Communications*, vol. 185, no. 10, pp. 2609–2621, 2014.

[2] A. Colagrossi, B. Bouscasse, M. Antuono, and S. Marrone, "Particle packing algorithm for SPH schemes," *Computer Physics Communications*, vol. 183, no. 2, pp. 1641–1683, 2012.

[3] Lind, S.J. and Xu, R. and Stansby, P.K. and Rogers, B.D., "Incompressible smoothed particle hydrodynamics for free-surface flows: A generalised diffusion-based algorithm for stability and validations for impulsive flows and propagating waves," *Journal of Computational Physics*, vol. 231, no. 4, pp. 1499–1523, 2012.

[4] N. Tsuruta, A. Khayyer, and H. Gotoh, "A short note on Dynamic Stabilization of Moving Particle Semi-implicit method," *Computers & Fluids*, vol. 82, pp. 158–164, 2013.

[5] A. Khayyer, H. Gotoh, and Y. Shimizu, "Comparative study on accuracy and conservation properties of two particle regularization schemes and proposal of an

optimized particle shifting scheme in ISPH context," *Journal of Computational Physics*, vol. 332, pp. 236–256, 2017.

[6] S. Marrone, A. Colagrossi, M. Antuono, G. Colicchio, and G. Graziani, "An accurate SPH modeling of viscous flows around bodies at low and moderate Reynolds numbers," *Journal of Computational Physics*, vol. 245, pp. 456–475, 2013.

[7] M. Antuono, A. Colagrossi, S. Marrone, and D. Molteni, "Free-surface flows solved by means of SPH schemes with numerical diffusive terms," *Computer Physics Communications*, vol. 181, no. 3, pp. 532–549, 2010.

[8] M. Antuono, A. Colagrossi, and S. Marrone, "Numerical diffusive terms in weakly-compressible SPH schemes," *Computer Physics Communications*, vol. 183, no. 12, pp. 2570–2580, 2012.

[9] P. Sun, A. Colagrossi, S. Marrone, and A. Zhang, "The $\delta plus$-SPH model: Simple procedures for a further improvement of the SPH scheme," *Computer Methods in Applied Mechanics and Engineering*, vol. 315, pp. 25–49, 2017.

[10] E. Rossi, A. Colagrossi, B. Bouscasse, and G. Graziani, "The Diffused Vortex Hydrodynamics method," *Communications in Computational Physics*, vol. 18, no. 2, pp. 351–379, 2015.

[11] Antuono, M and Marrone, S and Colagrossi, A and Bouscasse, B, "Energy balance in the δ-SPH scheme," *Computer Methods in Applied Mechanics and Engineering*, vol. 289, pp. 209–226, 2015.

[12] H. Wendland, "Piecewise polynomial, positive definite and compactly supported radial functions of minimal degree," *Adv. Comput. Math.*, vol. 4, no. 4, pp. 389–396, 1995.

[13] J. Monaghan and R. A. Gingold, "Shock Simulation by the particle method SPH," *Journal of Computational Physics*, vol. 52, no. 2, pp. 374–389, 1983.

[14] M. Antuono, B. Bouscasse, A. Colagrossi, and S. Marrone, "Energy conservation in the δ-SPH scheme," in *9th Int. SPHERIC workshop*, June, 3-5 2014.

[15] A. Colagrossi, M. Antuono, and D. Le Touzé, "Theoretical considerations on the free-surface role in the Smoothed-particle-hydrodynamics model," *Physical Review E*, vol. 79, no. 5, p. 056701, 2009.

[16] S. Marrone, A. Colagrossi, D. L. Touzé, and G. Graziani, "Fast free-surface detection and level-set function definition in SPH solvers," *Journal of Computational Physics*, vol. 229, no. 10, pp. 3652–3663, 2010.

[17] D. Le Touzé, A. Colagrossi, G. Colicchio, and M. Greco, "A critical investigation of smoothed particle hydrodynamics applied to problems with free-surfaces," *International Journal for Numerical Methods in Fluids*, vol. 73, no. 7, pp. 660–691, 2013.

[18] I. Federico, S. Marrone, A. Colagrossi, F. Aristodemo, and M. Antuono, "Simulating 2D open-channel flows through an SPH model," *European Journal of Mechanics-B/Fluids*, vol. 34, pp. 35–46, 2012.

[19] F. Maciá, M. Antuono, L. M. González, and A. Colagrossi, *Progress of Theoretical Physics*, vol. 125, no. 6, p. 1091, 2011.

[20] L. Chiron, G. Oger, D. Le Touzé, and M. De Leffe, "Improvements on particle refinement method with SPH," in *11th International SPHERIC Workshop*, June, 13-16 2016.

[21] B. Bouscasse, A. Colagrossi, S. Marrone, and M. Antuono, "Nonlinear water wave interaction with floating bodies in SPH," *Journal of Fluids and Structures*, vol. 42, pp. 112–129, 2013.

[22] D. Durante, E. Rossi, A. Colagrossi, and G. Graziani, "Numerical simulations of the transition from laminar to chaotic behaviour of the planar vortex flow past a circular cylinder," *Communications in Nonlinear Science and Numerical Simulation*, vol. 48, pp. 18–38, 2017.

[23] G.-J. Dong and X.-Y. Lu, "Characteristics of flow over traveling wavy foils in a side-by-side arrangement," *Physics of Fluids*, vol. 19, no. 5, p. 057107, 2007.

[24] J. Videler, *Fish swimming*, ser. Fish and Fisheries Serie 10. Springer, 1993.